Electron correlation effects on SiC(111) and SiC(0001) surfaces

2004 J. Phys.: Condens. Matter 16 S1721

(http://iopscience.iop.org/0953-8984/16/17/014)

INSTITUTE OF PHYSICS PUBLISHING JOURNAL OF PHYSICS: CONDENSED MATTER

J. Phys.: Condens. Matter **16** (2004) S1721–S1732 PII: S0953-8984(04)65097-1

Electron correlation effects on SiC(111) and SiC(0001) surfaces

F Bechstedt[1] **and J Furthmüller**

Friedrich-Schiller-Universität, Institut für Festkörpertheorie und Theoretische Optik, Max-Wien-Platz 1, 07743 Jena, Germany

E-mail: bech@ifto.physik.uni-jena.de

Received 23 June 2003
Published 16 April 2004
Online at stacks.iop.org/JPhysCM/16/S1721
DOI: 10.1088/0953-8984/16/17/014

Abstract

The possibility is discussed that, independent of the polytype, large electronic correlation effects give rise to semiconducting SiC surfaces with [111] or [0001] orientations. The most important surface translational symmetries $(\sqrt{3}\times\sqrt{3})$R30° and 3×3 are considered. The discussion is based on the detailed knowledge of the surface atomic geometries and the electronic structures derived for these geometries using a local density approximation for exchange and correlation. It is argued that the resulting half-filled, weakly dispersive dangling-bond bands within the fundamental gaps are split according to a Hubbard interaction parameter U, and that the surface systems undergo a Mott–Hubbard transition. Such a physical picture provides a qualitatively correct account of the single-particle excitation spectra either inferred from angle-resolved photoemission and inverse photoemission experiments or obtained from scanning tunnelling spectroscopy. The gap opening and hence the Hubbard U parameter are discussed in terms of their dependence on the surface reconstruction as well as the SiC polytype.

1. Introduction

Silicon carbide (SiC) exhibits the interesting property of polytypism [1]. It crystallizes in various crystal structures, e.g. the cubic (C) zinc-blende polytype 3C and hexagonal (H) polytypes nH or rhombohedral (R) polytypes nR with nSi–C bi-layers in the unit cell [2]. The most extreme polytypes are zinc-blende SiC (3C) with pure cubic stacking of the Si–C double layers in the [111] direction and wurtzite SiC (2H) with pure hexagonal stacking in the [0001] direction. The other polytypes represent hexagonal or rhombohedral combinations

[1] Author to whom any correspondence should be addressed.

of these stacking sequences [1]. The most important examples are 4H- and 6H-SiC with four (six) double layers and, hence, eight (twelve) atoms in the corresponding hexagonal unit cell.

Although the different polytypes are nearly degenerate energetically [3], their electronic properties vary remarkably. In particular, the excitonic energy gap varies from 2.4 eV for the zinc-blende structure (3C) to 3.3 eV for the wurtzite structure (2H) [4, 5]. This variation is accompanied by changes of the position of the conduction band minima in the three-dimensional Brillouin zone (BZ) [6, 7]. The considerable variation of the fundamental energy gaps and positions of the band extrema opens up the prospect of electronic heterostructures without lattice mismatches [8, 9]. Indeed, controlled layer-by-layer growth in the [111] or [0001] direction, e.g. by molecular beam epitaxy (MBE), does not only allow the growth of different polytypes but also of heteropolytypic quantum well structures and superlattices. Recent solid-source MBE experiments [10, 11] clearly demonstrated the achievement of growth of different polytypes on certain SiC substrates under Si-stabilized growth conditions and well-defined temperatures.

Consequently, the more or less Si-rich Si-terminated SiC(111) surfaces of 3C-SiC and SiC(0001) surfaces of 4H/6H-SiC are extremely important. Independent of the polytype, these surfaces show two basic translational symmetries or reconstructions. They exhibit a well-ordered $(\sqrt{3} \times \sqrt{3})$R30° reconstruction as one of the intrinsic surface phases [12–14]. This structure is not the most Si-rich phase. The addition of Si atoms results in a transition to a 3×3 overlayer structure [12, 13, 15, 16]. Identification of the atomic geometry of the reconstructed SiC surfaces by both experimental studies [12–16] and total-energy calculations [15–17] is a complicated process, in particular for the 3×3 geometry.

In recent years, during the experimental and theoretical studies of the SiC(0001) and SiC(111) surfaces with $\sqrt{3} \times \sqrt{3}$ and 3×3 translational symmetries, a variety of surprising results has been found. This concerns not only the atomic structure of the unusual 3×3 reconstruction [15, 16] but also, in particular, the electronic states. Whereas the standard electronic-structure calculations using a local density approximation (LDA) predicted rather dispersionless half-filled dangling-bond-related bands within the fundamental energy gap [15–17], such a picture is contradicted by spectroscopic studies, such as angular-resolved photoemission spectroscopy (ARPES), k-vector-resolved inverse photoemission spectroscopy (KRIPES) or their combination [18–22], as well as scanning tunnelling spectroscopy (STS) [23, 24]. For the $\sqrt{3} \times \sqrt{3}$ case they indicate a fully occupied surface-state band which is about 1 eV above the valence-band maximum (VBM). For the 3×3 case this band is slightly shifted towards higher energies. For the hexagonal polytypes there is an empty surface-state band at about 3 eV above the VBM. This gives a surface-state gap of about 2 eV for $\sqrt{3} \times \sqrt{3}$ overlayers. This value is reduced to about 1.2 eV in the 3×3 case.

In this paper we discuss how the theoretical and experimental results can be unified in a generalized one-electron picture, but taking strong electron correlation effects into account. In a first step, the atomic structure of the $\sqrt{3} \times \sqrt{3}$ and 3×3 surfaces is clarified in section 2. The resulting dangling-bond-related bands and surface states are discussed in section 3. In section 4 we show that the electronic structure can be described accurately, assuming a Mott–Hubbard insulator. Finally, a brief summary is given in section 5.

2. Atomic geometry

Our structural considerations and the discussion of the electronic states are based on calculations performed within the framework of density functional theory (DFT) in the LDA. Explicitly, we use the Vienna *ab initio* simulation package, described elsewhere [25]. Ultra-soft pseudo-potentials [26] are used for carbon, silicon and hydrogen, which allow us to reduce

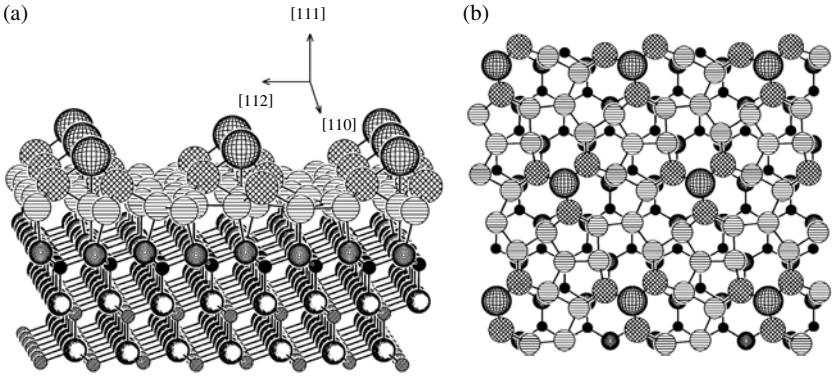

Figure 1. Perspective view on (a) and top view of (b) the Si-rich, Si-terminated SiC(111)3 × 3 surface within the tetramer-adlayer model. Dots designate C atoms. Large open (filled, hatched) circles designate Si atoms in the substrate (top-most substrate layer, adlayer). The larger hatched circles indicate Si atoms in the tetramer [15].

the cutoff in the plane-wave expansion to 13.2 Ryd. The surfaces are modelled by repeated slabs with 3×3 or $\sqrt{3} \times \sqrt{3}$ lateral unit cells. Each slab consists of six Si–C bi-layers and a vacuum region of the same thickness. The dangling bonds at the lower C-terminated half of the slab are saturated by hydrogen in order to avoid spurious interactions or electron transfers. Additional Si adatoms are allowed to cover the Si-terminated slab side. We use eight (four) $\boldsymbol{k}$ points to sample one half of the BZ of the $\sqrt{3} \times \sqrt{3}(3 \times 3)$ surface. In order to find the geometries, cubic stacking has been assumed along the [111] direction in each slab. We have shown [9, 26, 27] that the actual stacking is of minor influence on the surface geometry and energetics. However, in discussing the electronic structure we must take into account that the fundamental energy gap of 4H-SiC or 6H-SiC is about 1 eV larger than that of 3C-SiC. Calculating their band structures, the stacking of the slabs is changed according to the 4H or 6H arrangement. Another problem concerns underestimation of the gap within the DFT-LDA. Quasi-particle corrections must be taken into account [28, 29]. Their inclusion, however, almost corresponds to the application of a scissors operator of about 1 eV.

The ground state of the surfaces is evaluated by means of total-energy optimizations. All atomic coordinates in the upper half of the slab are relaxed until the Hellmann–Feynman forces vanish. Four different models, suggested by various authors [15, 20], have been used as initial configurations of the total-energy optimization in the 3×3 case. This number has been vastly increased for the $\sqrt{3} \times \sqrt{3}$ translational symmetry [9, 27]. Under very Si-rich preparation conditions, it is found that 3×3 translational symmetry is represented by a Si tetramer on a twisted Si adlayer with clover-like rings on top of the Si-terminated face [15, 16]. This structure is represented in figure 1. In other words, the 3×3 reconstruction includes a twisted Si adlayer above a bulk Si-terminated SiC substrate with a Si tetramer adcluster on top. With $\Theta = 13/9$, the Si coverage is larger than one monolayer. No stacking faults, dimers and corner holes appear.

The central element of the 3×3 reconstruction is a Si tetramer on top, consisting of a Si trimer and an additional Si adatom (figure 1(a)). The adatom cluster saturates nine of the 27 dangling bonds of the adlayer. The remaining dangling hybrids form a threefold coordination within the adlayer. There is a tendency for a rehybridization to sp^2 and p orbitals for one part of the adlayer atoms. Their sp^2 hybrids form bonds within the first adlayer, and the remaining p orbitals form bonds of the adlayer atoms to the substrate. The adlayer atoms that possess one bond to the trimer basis of the adcluster exhibit a tendency towards two sp and two p orbitals.

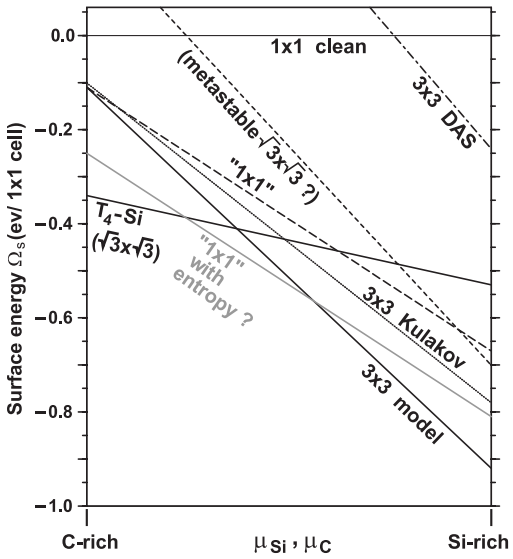

Figure 2. A phase diagram of an Si-terminated SiC(111) surface as a function of the chemical potential of the Si or C atoms. Relevant reconstruction models have been selected. The energy of the rather disordered 1×1 structure has been lowered by an entropy term, assuming that $S_s = 0.15\, k_B$ and $T = 1000$ K, in order to explain the sequence of phase transitions $\sqrt{3} \times \sqrt{3} \rightarrow 1 \times 1 \rightarrow 3 \times 3$ with increasing Si coverage [15].

The adatom itself appears to be unhybridized and bonded by p orbitals, as judged from its bond angles of 90°. Effectively, this allows an energetically favourable, almost s-like dangling bond or orbitals which, however, are only half-filled.

Under less Si-rich preparation conditions, a $\sqrt{3} \times \sqrt{3}$ structure is favoured. This is clearly demonstrated by the phase diagram in figure 2 [15], which shows the surface energy versus the chemical potential of silicon (or carbon). A minimization of the number of dangling bonds is achieved easily, however, just by adding a threefold coordinated adatom. This could be an atom that is chemically identical to a bulk species—here a Si atom because of the Si-rich preparation conditions. Such adatoms on (111) and (0001) surfaces may occupy two types of sites. These geometries are distinguished as hollow (H_3) and top sites (T_4), depending on whether the substrate atom below the adatom is found in the fourth or second atomic layer, respectively. In each of the geometries the adatom is in a threefold (3) symmetric site. In the T_4 case, a weak interaction of the adatom and the second-layer atom below occurs which gives almost a fourfold (4) coordination. There is consensus that this structure is formed by a T_4 adatom on top of the uppermost bulk-like Si layer [17, 27]. Such an adatom structure is shown in figure 3. The calculations demonstrate that the T_4 adsorbate site is much favoured over the H_3 site. However, this geometry still gives rise to dangling-bond-related surface states in the fundamental gap. The topmost dangling bond, localized at the Si adatom (see figure 4), is half-filled in such a simplified picture.

3. Band structures within DFT-LDA

The DFT-LDA band structures that result for the two reconstructions $(\sqrt{3} \times \sqrt{3})$R30° and 3×3 are plotted in figures 6 and 7 [20] versus high-symmetry lines in the corresponding BZ (figure 5). For both reconstructions, a well-pronounced dangling-bond-related band is

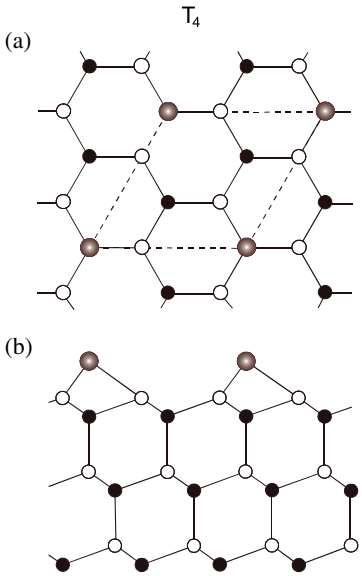

Figure 3. Si adatoms in a T_4 position on a SiC(111)($\sqrt{3} \times \sqrt{3}$)R30° surface. Open (filled) circles indicate Si (C) atoms. Adatoms are shaded. A top view (a) and a side view (b) are shown. A possible unit cell is indicated by the dashed lines.

(This figure is in colour only in the electronic version)

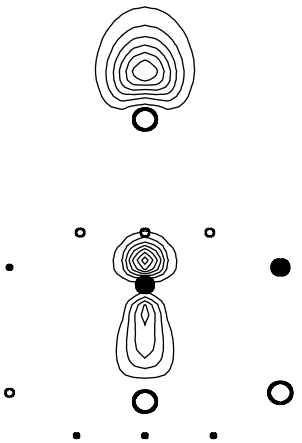

Figure 4. A dangling-bond state at the T_4-site Si atom. Plotted in greater detail is the squared wavefunction belonging to the corresponding band at the M point (see figure 5) of the surface BZ for the SiC(111)$\sqrt{3} \times \sqrt{3}$.

observed in either the upper part of the projected fundamental gap of 3C-SiC or the central part in the case of 6H-SiC or 4H-SiC. According to the electron-counting rule, this band pins the Fermi level. It is half filled, since there is only one dangling bond per surface unit cell. The bands are mostly related to the almost s-like orbitals that are localized at the adatoms for $\sqrt{3} \times \sqrt{3}$ or at the topmost atom of the adatom cluster in the 3×3 case. The general behaviour (i.e. the energetic position and the band dispersion) of the $\sqrt{3} \times \sqrt{3}$-related dangling-bond (figure 4) band is in agreement with other calculations [17, 30].

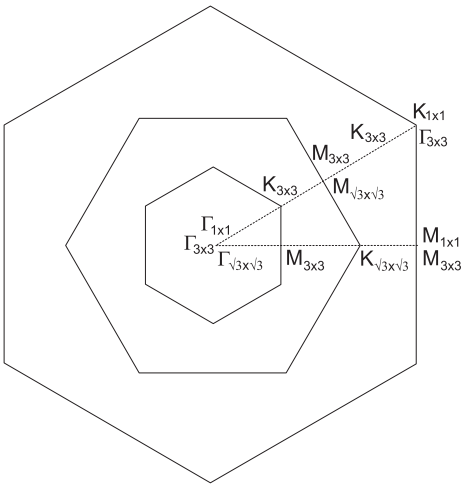

Figure 5. BZs for 3×3, $\sqrt{3} \times \sqrt{3}$ and 1×1 reconstructions. High-symmetry points and directions are indicated.

In the case of both reconstructions, the dangling-bond-related half-filled surface bands in figures 5 and 6 exhibit an extremely small dispersion, which is in agreement with the large adatom distances $D = 9.19$ Å (3×3) or 5.31 Å ($\sqrt{3} \times \sqrt{3}$). For 3C-SiC substrates, the bandwidths amount to 0.13 and 0.40 eV. The band maximum is located at the K (Γ) point, whereas the band minimum occurs at the Γ (K) point in the case of the 3×3 ($\sqrt{3} \times \sqrt{3}$) phase. For the smaller reconstruction $\sqrt{3} \times \sqrt{3}$, these findings and the bandwidth are in agreement with other DFT-LDA calculations [17, 30], except that the absolute position of the dangling-bond band is slightly higher with respect to the valence-band maximum due to the 6H substrate considered there. For instance, for 6H-SiC(0001)$\sqrt{3} \times \sqrt{3}$, a calculation using different pseudo-potentials and basis functions for expansion of the wavefunctions [30] yields a dangling-bond-related band with a bandwidth of 0.45 eV that disperses between 1.15 and 1.6 eV above the VBM. The Fermi level in this calculation is at 1.3 eV. Our calculations for 6H-SiC(0001)$\sqrt{3} \times \sqrt{3}$ confirm the bandwidth of about 0.45 eV. However, we find a position of the dangling-bond-related band of 6H-SiC(0001)$\sqrt{3} \times \sqrt{3}$ between 1.3 and 1.75 eV above the VBM, i.e. about 0.15 eV higher in energy than in [30]. This may be a consequence of the different alignment procedures that were used to plot simultaneously the surface bands and the projected bulk band structures in figure 6.

The dangling bonds are arranged in hexagonal lattices. Considering only the nearest-neighbour interaction of these dangling bonds, which may be characterized by a hopping parameter t, an analytical formula can be derived for the band dispersion $\varepsilon(\boldsymbol{k})$ [20, 31]. The diagonalization of the corresponding tight-binding Hamiltonian gives a dangling-bond band with a dispersion

$$\varepsilon(\boldsymbol{k}) = \begin{cases} 2t[1 + 2\cos(\pi s)] & \text{along } \Gamma\text{M} \\ 2t\left[2\cos\left(\dfrac{2\pi}{3}s\right) + \cos\left(\dfrac{4\pi}{3}s\right)\right] & \text{along } \Gamma\text{K} \end{cases} \tag{1}$$

in the corresponding hexagonal BZ (see figure 5). The variable s ($0 \leqslant s \leqslant 1$) describes a variation of the corresponding wavevector along a high-symmetry line from the centre of the BZ to the BZ boundary. A fit to the dispersion of the dangling-bond band calculated within DFT-LDA yields a hopping parameter $t = 0.014$ eV ($t = 0.05$ eV) for the $3 \times 3(\sqrt{3} \times \sqrt{3})$

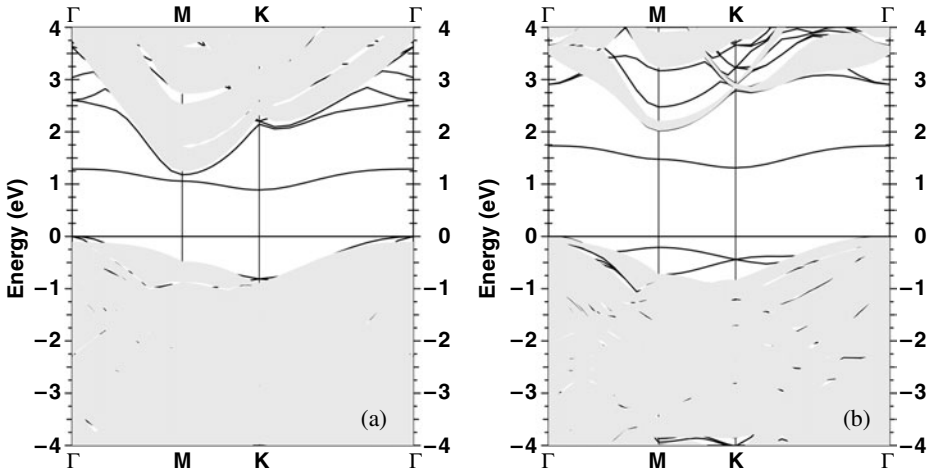

Figure 6. The electronic structures of the $\sqrt{3} \times \sqrt{3}$ reconstructed surfaces of (a) 3C-SiC(111) and (b) 6H-SiC(0001) within DFT-LDA. The projected bulk band structures are shown as shaded regions, whereas lines represent bands of surface bound states. The valence-band maximum is taken to be energy zero.

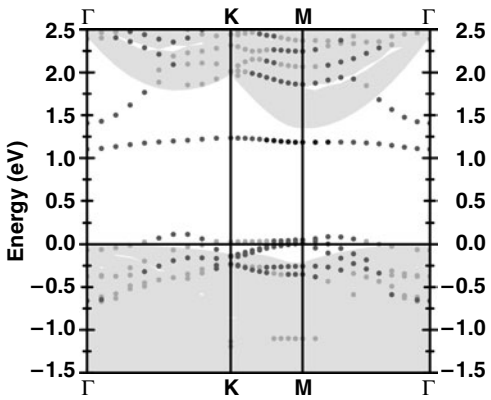

Figure 7. The band structure of the 3C-SiC(111)3 × 3 surface. The projected bulk band structure is shown by shaded regions; the dotted curves represent bands of surface bound states [20].

reconstruction of 3C-SiC(111). We mention that these parameters cannot be identified with those obtained for bulk systems. The hopping parameters differ by a factor of approximately three, which is in agreement with the variation of the hopping constant according to $1/D^2$ and the prefactors that usually give reasonable fits for bulk systems [31].

4. Mott–Hubbard picture and quasi-particle approach

The metallic nature of the dangling-bond-related surface bands in figures 6 and 7 is in clear contrast to the experimental findings [18–24]. For this reason, it has been suggested by Northrup and Neugebauer [32] and by Furthmüller *et al* [20] that a Mott–Hubbard transition may occur at these surfaces, resulting in a nonmetallic ground state. The extremely flat

dangling-bond-related bands indicate the possible effects of strong electron correlation and, hence, an important inhomogeneity of the corresponding electron gas. This has to be treated beyond the framework of the LDA for exchange and correlation.

To include strong correlation effects on electrons in the dangling-bond states at the top Si atoms of the adclusters (3×3) or T_4-site adatoms $(\sqrt{3}\times\sqrt{3})$, we consider a one-band Hubbard Hamiltonian for the half-filled band states [33]. The model is specified by the dispersion relation of the dangling-bond bands, $\varepsilon_{\mathrm{DB}}(\boldsymbol{k}) = \varepsilon_0 + \varepsilon(\boldsymbol{k})$, where ε_0 is a characteristic orbital energy of the isolated dangling bonds and $\varepsilon(\boldsymbol{k})$ is the dispersion given in equation (1). A nearest-neighbour hopping parameter t in a tight-binding picture (1) describes the interaction of the Si dangling bonds in different surface unit cells. The electron–electron interaction is retained by the on-site Coulomb integral U, which is the largest and not taken into account correctly within the local description of the DFT-LDA. Of course, the Coulomb interaction that is described by the integral is reduced due to the polarizability of the environment, in particular that of the substrate. We write the one-band Hubbard Hamiltonian in the form

$$H = \varepsilon_0 + t\sum_{i\neq j,\sigma} c^+_{i\sigma}c_{j\sigma} + U\sum_i c^+_{i\uparrow}c_{i\uparrow}c^+_{i\downarrow}c_{i\downarrow} \tag{2}$$

where the i and j sums run over the various (neighbouring) Si dangling orbitals and $\sigma = \uparrow$ and $\downarrow$ describe the spin orientation. An operator $c^+_{i\sigma}$ ($c_{i\sigma}$) creates (annihilates) an electron with spin σ on site i. The parameter U describes the effective Coulomb interaction between two electrons with opposite spin on the same Si dangling bond. Strong electron correlation means that this parameter is larger than the hopping parameter governing the bandwidth. We mention that Hamiltonians of type (2) have been employed in previous studies of two-dimensional arrays (with ferromagnetic or antiferromagnetic ordering) of Si dangling bonds on Si(111) surfaces [34–36].

The single-particle problem related to the Hamiltonian (2) cannot be solved exactly. When U is much larger than the bandwidth, an approximate solution results. Using the so-called Hubbard I decoupling of the two-particle Green function [37], the resulting quasi-particle bands are ($\sigma = \uparrow, \downarrow$)

$$\varepsilon_{\pm\sigma}(\boldsymbol{k}) = \varepsilon_0 + \tfrac{1}{2}\{\varepsilon(\boldsymbol{k}) + U \pm [(\varepsilon(\boldsymbol{k}) - U)^2 + 4\varepsilon(\boldsymbol{k})Un_{-\sigma}]^{\frac{1}{2}}\} \tag{3}$$

where the average occupation n_σ of the lattice sites with spin σ fulfils the conservation law $n_\uparrow + n_\downarrow = 1$. A two-dimensional translational symmetry must be assumed for the distribution of the electron spins over the surface. The dispersion $\varepsilon(\boldsymbol{k})$ without strong electron correlation is given in equation (1).

The bands in equation (3) depend on the spin configuration in the dangling bonds [37]. In the fully spin-polarized ferromagnetic configuration with $n_\uparrow = 1$ and $n_\downarrow = 0$ (or vice versa), only two bands with a finite spectral weight appear. They are

$$\begin{aligned}\varepsilon_{+\downarrow}(k) &= \varepsilon_0 + \varepsilon(\boldsymbol{k}) + U\\ \varepsilon_{-\uparrow}(k) &= \varepsilon_0 + \varepsilon(\boldsymbol{k})\end{aligned} \tag{4}$$

with $\varepsilon_{+\downarrow}(\boldsymbol{k})$ for the minority spin and $\varepsilon_{-\uparrow}(\boldsymbol{k})$ for the majority spin. The result (4) suggests that the short-range correlation effects are zero [37]. The paramagnetic state with $n_\uparrow = n_\downarrow = \frac{1}{2}$ should give the most realistic surfaces. The resulting bands keep the form (4). They can easily be discussed in the so-called atomic limit. For $U \gg \varepsilon(\boldsymbol{k})$, the asymptotic solutions also describe two bands:

$$\begin{aligned}\varepsilon_{+}(\boldsymbol{k}) &= \varepsilon_0 + \tfrac{1}{2}\varepsilon(\boldsymbol{k}) + U\\ \varepsilon_{-}(\boldsymbol{k}) &= \varepsilon_0 + \tfrac{1}{2}\varepsilon(\boldsymbol{k})\end{aligned} \tag{5}$$

independent of the spin orientation. Strong short-range correlation effects due to the Hubbard interaction U occur. In going from the one-electron model—as, for example, given by the DFT-LDA—to the Hubbard model, the doubly degenerate band $\varepsilon_{\mathrm{DB}}(\boldsymbol{k}) = \varepsilon_0 + \varepsilon(\boldsymbol{k})$ is replaced by two narrower bands which are separated by the energy U. The strong electron correlation effects open an energy gap which is proportional to U between the two bands $\varepsilon_+(\boldsymbol{k})$ and $\varepsilon_-(\boldsymbol{k})$ (equation (5)) that can be either completely empty or fully occupied. Indeed, the system undergoes a metal–insulator transition—a so-called Mott–Hubbard transition [38–40]. Compared to the correlation-free case, both bands (5) are at the same centre-of-gravity position, separated by U, but the dispersion of each band has been reduced to a half of its original value.

The parameters ε_0 and t of the bands in equation (5) are taken from the underlying DFT-LDA calculation. The parameter U is the energy required to remove one electron from an isolated dangling bond DB and add it to another dangling hybrid situated at an adatom ($\sqrt{3} \times \sqrt{3}$) or a top atom of a cluster (3×3). It is equal to the energy of the electronic transition $2DB(0) \rightarrow DB(+) + DB(-)$, where 0, + or − denote the charge states of the dangling bond DB. Therefore, it is also possible to estimate the effective interaction parameter U by means of total-energy differences between different occupations (charge states) of the dangling-bond bands within the framework of DFT-LDA calculations. Using such a delta-self-consistent field (ΔSCF) method [41, 42], it holds that $U = E(+) + E(-) - 2E(0)$, where $E(+)$, $E(-)$ and $E(0)$ represent the ground-state energies of a positively charged, negatively charged, and neutral supercell, respectively. The charges must be localized at the dangling bonds, giving rise to the surface band of interest.

The latter requirement poses a practical problem for ΔSCF calculations on these surfaces. The strong shifts of the eigenvalues of the dangling-bond-related bands, which are as large as U itself, may shift them into the valence or conduction bands. In particular, the small distance of the dangling-bond-related band with respect to the conduction band minimum creates a very critical situation not only for 3C-SiC(111) but even in the case of 6H-SiC(0001). Since a shift into the bulk bands would result in incorrect band occupation, we must avoid this. The only safe approach is to restrict it to fractional charges $+Qe$ and $-Qe$, where $|Q|$ is not larger than the distance of the dangling-bond-related band to the bulk band edges divided by the expected U parameter (typically, $|Q| = 0.1$–0.2 should not be exceeded). In this case it holds that $UQ^2 = E(+Q) + E(-Q) - 2E(0)$, with the well-known limiting case for $Q = 1$. Since the quadratic behaviour requires high accuracies for small values of Q, an even more desirable approach is to calculate the shift of the eigenvalue ε_0 of the dangling-bond-related band with respect to the vacuum level as a function of the charge Qe. This shift is given by QU and is linear in Q and hence numerically less critical. Nevertheless, the precise alignment of the vacuum level is spoiled by weak electric fields limiting the overall accuracy to about 0.1 eV. Using this procedure, it holds that simply $2UQ = \varepsilon(-Q) - \varepsilon(+Q)$, in the spirit of numerical differentiation by means of central differences. In addition—in all cases where the negative charging poses serious problems due to the small distance of the dangling-bond-related band to the conduction band—one can also use the expression $UQ = \varepsilon(0) - \varepsilon(+Q)$.

From the DFT-LDA eigenvalue shifts (as well as with a limited accuracy from total-energy differences [20]), one estimates a value of $U \approx 2.1$ eV ($U \approx 1.0$ eV) for the 3C-SiC(111)$\sqrt{3} \times \sqrt{3}$ (3×3) surface. For 6H-SiC(0001)$\sqrt{3} \times \sqrt{3}$, we estimate a slightly larger value of $U \approx 2.3$ eV, indicating a weak polytype dependence which is, however, not larger than the principal numerical accuracy. Unfortunately, the calculation of the total energies and eigenvalues of charged supercells suffers strongly from spurious electrostatic interactions between the supercells. Even fractional charges Q do not help, since the corresponding effects (i.e. the change of total energies proportional to the square of the charge and eigenvalue shifts linear in the charge) scale in the same way as the errors, and the relative error remains constant.

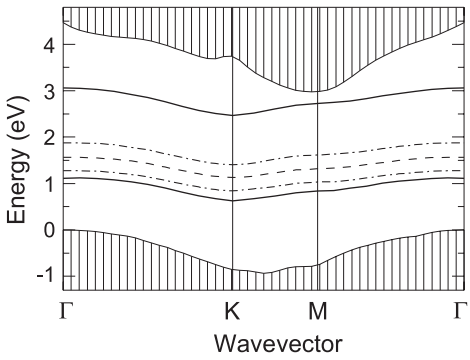

Figure 8. The quasi-particle band structure (solid curves and hatched regions) of the 6H-SiC(0001)$\sqrt{3} \times \sqrt{3}$ surface, calculated in a fully spin-polarized GW approximation. For comparison, the dangling-bond-related bands in DFT-LDA (dashed curve) or DFT-LSDA (dot–dashed curves) are also shown (from [46]).

Hence, the values represent a rather crude estimate (in particular for $\sqrt{3} \times \sqrt{3}$). For the more Si-rich 3×3 surface, the value of U approaches more closely that of pure Si due to the larger Si coverage of this structure and, hence, increased screening. Using a similar method, Northrup and Neugebauer [32] calculated a value of $U = 1.6$ eV for the 6H-SiC(0001)$\sqrt{3} \times \sqrt{3}$ surface. Other authors found $U = 1.8$ eV [43]. The experimental values for the gap are 2.0 eV for 6H-SiC(0001)$\sqrt{3} \times \sqrt{3}$ [19, 23] and 1.0 eV [22] or 1.2 eV [24] for 6H-SiC(0001)3×3. Recently, a value of $U = 2.2 \pm 0.2$ eV has been derived for 4H-SiC(0001)$\sqrt{3} \times \sqrt{3}$ [44].

The values of U may also be estimated from the Coulomb repulsion and the screening response to charge transfers. A rough estimate of the Hubbard parameter U follows from the orbital properties and the electronic polarization that is induced in the surroundings of the dangling bond by an additional electron. It almost holds that $U = U^{\text{atom}}/\varepsilon_{\text{eff}}$, where U^{atom} is the atomic value and ε_{eff} is the electronic dielectric constant of the effective medium. In the solid-state table of Harrison, one finds the value $U^{\text{atom}} = 7.64$ eV for an isolated Si sp^3 hybrid [45]. The effective dielectric constant of a surface may be determined by the mean value $\varepsilon_{\text{eff}} = \frac{1}{2}(\varepsilon_{\text{b}} + 1)$ of the bulk and vacuum constants. For SiC with $\varepsilon_{\text{b}} = 6.7$ [31], an effective interaction parameter of approximately $U \approx 2$ eV is estimated. For more Si-rich environments, e.g. for Si surfaces with $\varepsilon_{\text{b}} = 12$, values of the effective Coulomb interaction slightly larger than $U = 1$ eV are predicted.

Since, without spin polarization, the dangling-bond band is half-filled, another possibility exists to obtain the band structure given in (3)–(5) via an *ab initio* mean-field approach [46]. It is necessary to accurately incorporate the long-range correlation and screening effects in the electronic self-energy operator for exchange and correlation. This can be done in a highly reliable way by using the GW approximation [28]. However, as a basis for the GW calculation, one must first treat the surface system within the local spin-density approximation (LSDA) to obtain the fully spin-polarized configuration. Already, this leads to a splitting of the former metallic DFT-LDA band (figure 8, dashed curve) into two bands separated by a direct DFT-LSDA gap of 0.6 eV for $\sqrt{3} \times \sqrt{3}$ (see figure 8, dot–dashed curves) [46]. The resulting quasi-particle bands (figure 8, solid curves) are split further. Compared to the lower DFT-LSDA band, for 6H-SiC(0001)$\sqrt{3} \times \sqrt{3}$ the occupied majority-spin band is shifted downwards by 0.2 eV to lower energies, while the empty minority-spin band is shifted upwards by 1.15 eV to higher energies. This is accompanied by a slight increase of the bandwidths. The mean direct gap between the two bands is increased by 1.35 eV due to the quasi-particle corrections

and amounts to 1.95 eV in total. This value is in good agreement with the on-site-interaction parameter U of the Hubbard model, calculated using the ΔSCF method [20].

One remark is necessary. At a real SiC(0001) surface, the spin configuration may not be fully polarized. In fact, within the DFT-LSDA calculation the total energy of the spin-polarized surface is nearly the same as that of the unpolarized surface. It can thus be expected that the spin polarization, if favourable at all, is easily broken by nonzero temperature or other perturbations, so it seems likely that the real surface is not spin polarized.

5. Summary

The apparent discrepancy between experiment and theory concerning the nonmetallic or metallic nature of the $\sqrt{3} \times \sqrt{3}$- and 3×3-reconstructed Si-terminated SiC surfaces can be solved after the inclusion of strong electron correlation effects. The energy gaps in the band structure of 6H-SiC(0001)$\sqrt{3} \times \sqrt{3}$ (about 2 eV) and 6H-SiC(0001)3×3 (about 1 eV) surfaces are understandable. The results obtained by combination of photoemission and inverse photoemission studies or by scanning tunnelling spectroscopy are real. The inclusion of exchange and correlation effects in the theory beyond the LDA gives rise to a splitting of the dangling-bond-related bands within the projected bulk fundamental gaps of the polar SiC surfaces, independent of the polytype. Since the dispersion of these bands is small (more strictly, since their bandwidths are small compared to the characteristic parameter U of the electron correlation in such dangling bonds), the validity of the Mott–Hubbard picture can be shown. Because of the strong electron correlation, the surface systems considered undergo a Mott–Hubbard transition. We note that indications for a similar effect (a gap free of surface states around the Fermi level and an occupied surface band) have recently been observed for an especially prepared 6H-SiC(0001)1×1 surface [47] (also see the article by Seyller [48] in this topical issue).

Acknowledgments

This work was supported financially by the Deutsche Forschungsgemeinschaft (SFB 196, Project A8) and the EU Research Training Network NANOPHASE (HPRN-CT-2000-00167).

References

[1] Verma A R and Krishna P 1966 *Polymorphism and Polytypism in Crystals* (New York: Wiley)
[2] Ramsdell R S 1947 *Am. Mineral.* **32** 64
[3] Käckell P, Wenzien B and Bechstedt F 1994 *Phys. Rev.* B **50** 17037
[4] Choyke W J, Hamilton D R and Patrick L 1964 *Phys. Rev.* A **133** 1163
[5] Choyke W J 1990 *The Physics and Chemistry of Carbides, Nitrides and Borides* (*NATO ASI Series E vol 185: Applied Sciences*) ed R Freer (Dordrecht: Kluwer) p 563
[6] Käckell P, Wenzien B and Bechstedt F 1994 *Phys. Rev.* B **50** 10761
[7] Bechstedt F 1998 *Mater. Sci. Forum* **264–268** 265
[8] Bechstedt F and Käckell P 1995 *Phys. Rev. Lett.* **75** 2180
[9] Bechstedt F, Käckell P, Zywietz A, Karch K, Adolph B, Tenelsen K and Furthmüller J 1997 *Phys. Status Solidi* b **202** 35
[10] Fissel A, Schröter B, Kaiser U and Richter W 2000 *Appl. Phys. Lett.* **77** 2418
[11] Fissel A, Kaiser U, Schröter B, Richter W and Bechstedt F 2001 *Appl. Surf. Sci.* **184** 37
[12] Kaplan R 1989 *Surf. Sci.* **215** 11
[13] Li L, Hasegawa Y, Tsong I S T and Sakurai T 1996 *J. Physique Coll.* **6** C5 167
[14] Owman F and Martensson P 1995 *Surf. Sci.* **330** L639

[15] Furthmüller J, Käckell P, Bechstedt F, Fissel A, Pfennighaus K, Schröter B and Richter W 1998 *J. Electron. Mater.* **27** 848
[16] Starke U, Schardt J, Bernhardt J, Franke M, Reuter K, Wedler H, Heinz K, Furthmüller J, Käckell P and Bechstedt F 1998 *Phys. Rev. Lett.* **80** 758
[17] Northrup J E and Neugebauer J 1995 *Phys. Rev.* B **52** 17001
[18] Johansson L I, Owman F and Martensson P 1996 *Surf. Sci.* **360** L478
[19] Themlin J-M, Forbeaux I, Langlais V, Belkhir H and Debever J-M 1997 *Europhys. Lett.* **39** 61
[20] Furthmüller J, Bechstedt F, Hüsken H, Schröter B and Richter W 1998 *Phys. Rev.* B **58** 13712
[21] Benesch C 1998 *PhD Thesis* Westfälische Wilhelms-Universität, Münster
[22] Johansson L S O, Buda L, Laurensis M, Krieftewirth M and Reihl B 2000 *Surf. Sci.* **445** 109
[23] Ramachandran V and Feenstra R M 1999 *Phys. Rev. Lett.* **82** 1000
[24] Gasparov V A, Riehl-Chudoba M, Schröter B and Richter W 2000 *Europhys. Lett.* **51** 527
[25] Kresse G and Furthmüller F 1996 *Comput. Mater. Sci.* **6** 15
Kresse G and Furthmüller F 1996 *Phys. Rev.* B **54** 11169
[26] Furthmüller J, Käckell P, Bechstedt F and Kresse G 2000 *Phys. Rev.* B **61** 4576
[27] Käckell P, Furthmüller J and Bechstedt F 1997 *Diamond Relat. Mater.* **6** 1346
[28] Wenzien B, Cappellini G and Bechstedt F 1995 *Phys. Rev.* B **51** 14071
[29] Wenzien B, Käckell F, Bechstedt F and Cappellini G 1995 *Phys. Rev.* B **52** 10897
[30] Sabisch M, Krüger P and Pollmann J 1997 *Phys. Rev.* B **55** 10561
[31] Harrison W A 1989 *Electronic Structure and the Properties of Solids* (New York: Dover)
[32] Northrup J E and Neugebauer J 1998 *Phys. Rev.* B **57** R4230
[33] Jones W and March N H 1985 *Theoretical Solid State Physics* (New York: Dover)
[34] Allan G and Lannoo M 1977 *Surf. Sci.* **63** 11
[35] Duke C B and Ford W 1981 *Surf. Sci.* **111** L685
[36] Del Sole R and Chadi D J 1981 *Phys. Rev.* B **24** 7430
[37] Hubbard J 1963 *Proc. R. Soc.* A **276** 238
Hubbard J 1964 *Proc. R. Soc.* A **281** 401
[38] Mott N F 1949 *Proc. R. Soc.* A **62** 416
[39] Ashcroft N W and Mermin N D 1976 *Solid State Physics* (Philadelphia, PA: Saunders)
[40] Santoro G, Scandolo S and Tosatti E 1999 *Phys. Rev.* B **59** 1891
[41] Jones R O and Gunnarsson O 1989 *Rev. Mod. Phys.* **61** 689
[42] Godby R W and White I D 1997 *Phys. Rev. Lett.* **79** 1770
[43] Lu W, Krüger P and Pollmann J 2000 *Mater. Sci. Forum* **338–342** 349
[44] Ostendorf R, Benesch C and Zacharias H 2003 *Verh. Dtsch. Phys. Ges.* **38** 445
[45] Harrison W A 1999 *Elementary Electronic Structure* (Singapore: World Scientific)
[46] Rohlfing M and Pollmann J 2000 *Phys. Rev. Lett.* **84** 135
[47] Sieber N, Seyller T, Ley L, Polcik M, James D, Ridley J D and Leckey R C G 2002 *Mater. Sci. Forum* **389–393** 713
[48] Seyller T 2004 *J. Phys.: Condens. Matter* **16** S1755